End Concrete Cover Separation in RC Structures Strengthened in Flexure with NSM FRP: Analytical Design Approach

Mohammadali Rezazadeh [1], Joaquim A. O. Barros [2], Honeyeh Ramezansefat [3],

ABSTRACT

Fiber-reinforced-polymer (FRP) composite materials applied according to the near-surface-mounted (NSM) technique are very effective for the flexural strengthening of reinforced-concrete (RC) structures. However, the flexural strengthening effectiveness of this NSM technique is sometimes compromised by end concrete cover separation (CCS) failure, which is a premature failure before occurring the conventional flexural failure modes. Due to the complexity of this failure mode, no analytical approach, with a design framework for its accurate prediction, was published despite the available experimental results on this premature failure. In the present study, a novel simplified analytical approach is developed based on a closed form solution for an almost accurate prediction of CCS failure in RC structures strengthened in flexure with NSM FRP reinforcement. After demonstrating the good predictive performance of the proposed model, it was used for executing parametric studies in order to evaluate the influence of the material properties and FRP strengthening configuration on the susceptibility of occurring the CCS failure. At the end, regarding to the FRP strengthening configuration, some design recommendations were proposed to maximize the resistance of NSM FRP strengthened structures to the susceptibility of occurring the CCS failure.

Keywords: Analytical approach, concrete cover separation, FRP composite materials, NSM technique.

[1] ISISE, PhD of the Structural Division of the Dep. of Civil Engineering, University of Minho, 4800-058 Guimarães, Portugal. rzh.moh@gmail.com

[2] ISISE, Full Professor of the Structural Division of the Dep. of Civil Engineering, University of Minho, 4800-058 Guimarães, Portugal. barros@civil.uminho.pt

[3] ISISE, Postdoctoral Researcher of the Structural Division of the Dep. of Civil Engineering, University of Minho, 4800-058 Guimarães, Portugal. honeyrscivil@gmail.com

1. Introduction

Fiber reinforced polymer (FRP) composite materials applied according to the externally bonded (EB) and near surface mounted (NSM) techniques are now routinely used for the strengthening purposes of reinforced concrete (RC) structures [1-5]. In the context of NSM technique, in order to provide a higher FRP reinforcement ratio for the flexural strengthening of RC structures, two possibilities can be adopted: 1) using the FRP strips of larger cross sectional area; 2) increasing the number of FRP strips. Regarding to the first possibility, available research evidenced that the pullout load capacity of NSM FRP strips is increased with the use of FRP strips of the larger cross section depth, as well as installation of the FRP strips into deeper grooves [6]. However, the use of larger FRP depth according to NSM technique is limited by the concrete cover thickness of the tensile steel bars of RC structure. For exceeding this concrete cover thickness, the bottom arm of the steel stirrups needs to be cut. In this context, Costa and Barros (2009) experimentally investigated the influence, in terms of the beam's load carrying capacity, of cutting the bottom arm of steel stirrups for the installation of CFRP strips according to NSM technique [7]. The experimental results showed that cutting the bottom arm of steel stirrups in flexurally strengthened RC beams, which have a percentage of steel stirrups that avoids the shear failure, has a marginal impact in terms of the flexural strengthening effectiveness of the NSM technique. The effectiveness of other alternative, consisting on the increase of the number of NSM FRP strips, is limited by the detrimental interaction effect between two adjacent FRPs in the concrete substrate [6, 8]. In fact, when RC beams are strengthened with NSM FRP technique, an in-plane shear crack can be initiated at the extremities of the NSM FRP reinforcement due to high stress gradient caused by the abrupt termination of the FRP [1]. This crack is propagated along the depth of the concrete cover of the beam up to attain the tensile steel reinforcement level, and then progresses horizontally along this level due to the resistance offered by this reinforcement to the propagation of the crack through it (see Fig. 1) [8]. Furthermore, the concrete resistance at this level is relatively smaller than in the other parts, which can be attributed to the existence of a higher percentage of voids below the longitudinal tensile steel bars due to the concrete casting conditions in RC beams that can cause the formation of a weak plane in the concrete microstructure just below these bars [6, 7]. The weakness of this plane increases with the number of tensile bars. Propagation of the FRP-end section crack, horizontally along this weak plane, causes the formation of concrete cover separation (CCS) failure (also designated by rip-off, represented in Fig. 1), which is a premature failure of the NSM

FRP strengthened beams, since it occurs before the conventional flexural failure modes, with a detrimental consequence in the flexural strengthening effectiveness of the NSM technique. The susceptibility to CCS failure in NSM FRP strengthened beams is influenced by some variables, such as the concrete strength, reinforcement ratio of existing longitudinal steel bars, the relative position between the longitudinal steel and FRP reinforcements, number of FRP reinforcements, and distance between the consecutive FRPs [6].

On the other hand, existing research has shown that, despite the available experimental results on the CCS failure, few studies have been dedicated to propose a numerical strategy capable of predicting the behavior of RC beams strengthened using NSM FRP technique when failing by CCS failure [9-11]. Besides these numerical studies, for predicting the maximum flexural capacity of strengthened RC beams when CCS failure occurs at ultimate stage, developing a simplified analytical approach based on a closed form solution (by hand calculation without any programming help) is still a requirement for engineers and researchers with limited exposure to FRP design that needs to be addressed.

The present paper is dedicated to the development of a novel simplified analytical approach, with a design framework, capable of accurately predict the CCS failure in RC beams strengthened in flexure with NSM FRP reinforcement, by considering the influence of the effective parameters on the occurrence of this type of failure mode. After demonstrating the good predictive performance of the proposed analytical approach by predicting several relevant experimental tests, parametric studies were carried out to evaluate the influence of material properties and FRP strengthening configurations on the susceptibility of occurring the CCS failure. Finally, some recommendations in terms of FRP strengthening configurations using NSM technique are proposed to maximize the resistance of strengthened structures to the susceptibility of occurring the CCS failure.

2. Analytical approach

In the current section, a simplified analytical approach based on a closed form solution is developed with the aim of being a design proposal for engineers to predict the ultimate flexural capacity of a RC beam strengthened with NSM FRP reinforcement failing by concrete cover separation (CCS). According to this approach, the CCS failure is assumed to occur when the principal tensile stress transferred to the surrounding concrete at the extremity of the longitudinal

NSM FRP reinforcement attains the concrete tensile strength ($f_{ct} = 0.56\sqrt{f_c'}$, where f_c' is concrete compressive strength [12]). In this study, the shape of the tensile fracture surface of this surrounding concrete at the extremity zone of NSM FRPs was inspired on the works of [8, 13]. However, the concrete fracture body adopted in these literatures (a semi-pyramidal shape assuming NSM FRPs on the structure's surface) was modified in the current analytical approach in order to consider the influence of the NSM FRP installation depth from the beam's tensile surface on the susceptibility of occurring the CCS failure.

Furthermore, the present analytical approach is developed by considering the influence of the effective parameters (previously indicated) on the occurrence of the CCS failure mode. Fig. 2 schematically represents the geometry and reinforcement details of the simply supported strengthened beam adopted for this analytical study. Moreover, this strengthened beam is supposed to have a shear reinforcement ratio that avoids the shear failure. The beam is also assumed to be subjected to a four-point monotonic loading configuration, but other loading configurations can be adopted with straightforward adjustments due to the general character the model is formulated.

2.1. Assumptions

The following assumptions were adopted in the current analytical approach:

- Strain in the longitudinal steel bars, FRP reinforcement and concrete is directly proportional to their distance from the neutral axis of the cross section of the RC element;
- There is no slip between steel reinforcement and surrounding concrete;
- The possibility of occurring the FRP debonding failure is considered at the extremity zones of FRP bonded length (within the resisting bond length), while out of these FRP bonded zones, perfect bond condition is assumed between FRP and surrounding material.

2.2. Analytical model description

According to the developed analytical approach, the concrete cover separation failure is assumed to initiate when stress gradients in the concrete fracture surface at the extremities of the NSM FRP reinforcement attain the corresponding concrete tensile strength. The adopted shape for the concrete fracture surface at the extremity of each longitudinal NSM FRP reinforcement applied for the flexural strengthening on the beam's tensile surface is composed of a semi-pyramidal (the concrete part above the NSM FRP) and wedge (the concrete part below the NSM FRP) bodies (Fig. 3c). The dimensions of this concrete fracture shape are supposed to be limited by some restrictions to consider the influence of the effective variables on the susceptibility to the occurrence of CCS failure, and also to simplify the model. In order to determine the resistance of the surrounding concrete at the extremity zones of the NSM FRPs considering the assumed concrete fracture body, the slip between the NSM FRP reinforcement and its surrounding concrete is neglected along the height of the fracture semi-pyramidal (which is defined as the resisting bond length, L_{rb} in Fig. 3c). The resistance to the fracture of this concrete volume corresponding to each NSM FRP can be determined by considering the strength characteristics of concrete.

Furthermore, in this analytical approach, CCS is predicted by assessing the possibility of occurring the concrete fracture at the extremities of the FRP reinforcement in comparison with FRP debonding and rupture of the FRP failure modes (Fig. 3). Finally, the ultimate flexural capacity of a NSM FRP strengthened beam developing CCS failure can be determined using the maximum applicable force to all the NSM FRPs at the end section of the resisting bond length (L_{rb}).

The conditions for the occurrence of these three failure modes at the extremity zones of the longitudinal NSM FRP reinforcement are described in the following paragraphs.

Rupture of FRP Reinforcement

Tensile strength of the FRP reinforcement (F_{fu}) can be determined by the following equation:

$$F_{fu} = a_f . b_f . f_{fu} \tag{1}$$

where a_f and b_f are the thickness and height of FRP strip's cross section, and f_{fu} is the tensile strength of FRP. In the case of a round FRP bar, its cross section is converted to an equivalent square cross sectional area.

Resisting Bond Force

The maximum value of the force (F_{rb}) that can be transferable through the resisting bond length (L_{rb}) by the FRP strips can be obtained by Eq. (2) adopting an idealized local bond-slip relationship with a single softening branch as shown in Fig. 3b [13, 14].

$$F_{rb}(L_{rb}) = L_p.\frac{1}{J_1}.\lambda.\left\{C_1.\left[\cos\left(\lambda.L_{rb}\right)-1\right]-C_2.\sin\left(\lambda.L_{rb}\right)\right\}$$

where

$$L_p = 2.b_f + a_f \ ; \ J_1 = \frac{L_p}{\left(a_f.b_f\right)}.\left(\frac{1}{E_f}+\frac{\left(a_f.b_f\right)}{\left(A_c.E_c\right)}\right) \qquad (2)$$

$$\frac{1}{\lambda^2} = \frac{\delta_{\max}}{\left(\tau_{\max}.J_1\right)} \ ; \ C_1 = \delta_{\max} - \frac{\left(\tau_{\max}.J_1\right)}{\lambda^2} \ ; \ C_2 = -\frac{\left(\tau_{\max}.J_1\right)}{\lambda^2}$$

where E_f and E_c are the elasticity modulus of FRP and concrete, respectively; $\tau_{\max}$ and $\delta_{\max}$ are the maximum shear stress and maximum slip of the local bond stress-slip relationship, respectively; A_c is the cross sectional area of the surrounding concrete that provides confinement to each NSM FRP strip, and for outer-FRPs and inter-FRPs can be obtained by Eqs. (3)a and (3)b, respectively.

$$A_c = \min\left(2.s_f^{'} ; s_f\right).c_c \qquad (3)\text{a}$$

$$A_c = s_f.c_c \qquad (3)\text{b}$$

where s_f is the distance between two adjacent FRP strips; $s_f^{'}$ is the distance between the beam edge and the nearest FRP strip, and c_c is the concrete cover thickness beneath the longitudinal tensile steel bars (Figs. 2 and 4).

The maximum bond force (F_{rb}) corresponding to the resisting bond length (L_{rb}) should be limited to the maximum debonding resistance (F_{rbe}) and its corresponding effective resisting bond length (L_{rbe}) given by the following equations [13]:

$$L_{rbe} = \frac{\pi}{(2.\lambda)} \quad (4)a$$

$$F_{rbe} = \frac{\left(L_p.\lambda.\delta_{\max}\right)}{J_1} \quad (4)b$$

Concrete Fracture Capacity

Dimensions of the concrete fracture surface at the extremities of NSM FRPs are assumed to be limited by some geometric conditions in order to consider the effects, on the susceptibility for the occurrence of the CCS failure, of concrete weak plane just below the longitudinal steel bars, the relative position between the longitudinal steel and FRP reinforcements, number of NSM FRPs, and distance between consecutive FRPs. These conditions aim to minimize the interaction between the concrete fracture surfaces of consecutive FRP strips, as is represented in Fig. 4. Besides these conditions, another one is assumed to consider the possibility of occurring a weak plan just beneath the tensile steel bars. Regarding to this condition, the thickness of the concrete fracture body is limited to the concrete cover thickness beneath the longitudinal tensile steel bars (c_c) (see Fig. 4).

Accordingly, a boundary should be defined for the base area of the concrete fracture body (rectangular shape as represented in Fig. 3c) in order to consider these geometric conditions. This boundary, of rectangular shape for the base area of the concrete fracture body, limits the vertical and horizontal sides of this rectangle to a length of $s_c + l_f$ and $2s_c$, respectively, where s_c can be obtained as follows (see Figs. 4 and 5):

$$s_c = \min\left(s'_f \; ; s_f / 2 \; ; (c_c - l_f)\right) \le b/2 \quad (5)$$

in which l_f is the distance between the geometric center of FRP strip cross section and the beam's tensile surface, and can be obtained by $l_f = b_f/2 + e_c$, where e_c is the epoxy cover thickness beneath the FRP strip (see Fig. 2).

In fact, Eq. (5) is developed considering the outer-FRP strips (the two ones near the element's edges) (Fig. 4), while when more than two FRP strips are used for the strengthening application ($N > 2$, where N is the number of the

NSM FRP reinforcements), for the inner-FRP strips, this equation should be modified by neglecting the term of $s_f^{'}$. In this context, adopting a FRP strip for the strengthening application ($N = 1$), the term of $s_f / 2$ in Eq. (5) should be ignored.

The resisting bond length (L_{rb}) is obtained by:

$$L_{rb} = s_c / \tan\alpha \tag{6}$$

where α is the angle formed by the principal generatrices of the semi-pyramidal part of concrete fracture body with the FRP longitudinal axis (see Figs. 4 and 5). In the previous works, conducted by [8, 13], a constant value of 28.5º and 35º was adopted for this angle, respectively. However, in the current analytical approach, this angle is defined as a function of the boundary limits adopted for the concrete tensile fracture body in the NSM FRP strengthened beams, a subject to be treated in the next section.

The vertical eccentricity (y_c) of the FRP tensile force (F_f) to the centroid of the concrete fracture body creates an active moment ($M_f = F_f . y_c$), causing a concrete fracture initiated from the end section of the NSM FRP reinforcement (see Fig. 5). This vertical eccentricity (y_c) for the adopted geometry of the concrete fracture body can be obtained by Eq. (7), whose details are available in Appendix A.

$$y_c = (3.s_c^2 - 6.l_f^2) / (8.s_c + 12.l_f) \tag{7}$$

The tensile force transferred from the FRP to its surrounding concrete fracture body is locally supported by the resisting bending moment (M_r) formed by the resisting tensile force acting on the top surface (F_{ctv}) and shear force acting on the lateral vertical faces (T_s) of this body, as represented in Fig. 5. Since the CCS failure is initiated from the end section of the NSM FRP reinforcement, the distribution of these concrete tensile and shear stresses are supposed to be linear considering the corresponding maximum values at the FRP end section ($f_{ct} = 0.56\sqrt{f_c^{'}}$: concrete tensile strength; $\tau_s = 0.17\sqrt{f_c^{'}}$: concrete shear strength) and null value at the section corresponding to the resisting bond length (L_{rb}), represented in Fig. 5. Moreover, in this figure, the assumed linear distribution of the concrete tensile ($f_{ct(x)}$) and shear ($\tau_{s(x)}$) stresses is represented with respect to the corresponding concrete tensile strength and concrete shear strength, and the corresponding values at a distance of x from the end section of the FRP reinforcement are obtained from the following equations:

$$f_{ct(x)} = f_{ct} - (f_{ct}.x/l_t) \tag{8}$$

$$\tau_{s(x)} = \tau_s - (\tau_s.x/l_s) \tag{9}$$

where l_t and l_s are the slant length of the top and side faces of the concrete fracture body (Fig. 5), obtained by:

$$l_t = l_s = L_{rb}/\cos\alpha \tag{10}$$

Therefore, the concrete tensile resistance on the top slant area (F_{ct}) and shear resistance on the lateral vertical faces (T_s) of the fracture body are determined as follows:

$$F_{ct} = \int_0^{l_t} f_{ct(x)}.a_{(x)}.dx = s_c.f_{ct}.l_t/3 \tag{11)a}$$

where

$$a_{(x)} = 2.s_c.x/l_t \tag{11)b}$$

and

$$T_s = \int_0^{l_s} \tau_{s(x)}.b_{(x)}.dx = \tau_s.l_s.(l_f/2 + s_c/6) \tag{12)a}$$

where

$$b_{(x)} = l_f + (s_c.x/l_s) \tag{12)b}$$

Accordingly, the resisting bending moment (M_r) provided by the surrounding concrete at the section corresponding to the resisting bond length (L_{rb}) is obtained by:

$$M_r = F_{ctv}.\left(L_{rb} - x_t.\cos\alpha\right) + 2.T_s.\left(L_{rb} - x_s.\cos\alpha\right) \tag{13)a}$$

where

$$F_{ctv} = F_{ct}.\cos\alpha \tag{13)b}$$

and x_t and x_s are the distance of resultant point of F_{ct} and T_s applications from the FRP end section, respectively (see Fig. 5), and are calculated by:

$$x_t = \left(\int_0^{l_t} f_{ct(x)}.a_{(x)}.x.dx\right) \Big/ F_{ct} = l_t/2 \tag{14}$$

$$x_s = \left(\int_0^{l_s} \tau_{s(x)}.b_{(x)}.x.dx\right) \Big/ T_s = \left(l_f.l_s/3 + s_c.l_s/6\right) \Big/ \left(l_f + s_c/3\right) \tag{15}$$

Hence, the occurrence of the CCS failure can be expected when the FRP active moment (M_f) exceeds the surrounding concrete resisting moment (M_r). Consequently, the maximum allowable force ($F_{f(\max)}$) that can be applied to the NSM FRP reinforcement before occurring the CCS failure at the section corresponding to the resisting bond length (L_{rb}) is determined by:

$$M_f = M_r \rightarrow F_{f(\max)}.y_c = M_r \rightarrow F_{f(\max)} = M_r/y_c \tag{16}$$

On the other hand, according to the methodology of the proposed analytical approach, installing the NSM FRP reinforcement more far away from the beam's tensile surface (higher l_f) causes a reduction in terms of the FRP active moment (M_f), resulting in a higher resistance to the susceptibility of CCS failure. By increasing this FRP installation depth (l_f), the CCS failure cannot occur once the vertical eccentricity (y_c) of the FRP tensile force to the centroid of the concrete fracture body achieves a negative value ($y_c \le 0$), as follows:

$$y_c = (3.s_c^2 - 6.l_f^2) \big/ (8.s_c + 12.l_f) \le 0 \rightarrow (3.s_c^2 - 6.l_f^2) \le 0 \rightarrow s_c \le \sqrt{2}.l_f \tag{17}$$

Furthermore, in order to maximize the resistance to the occurrence of CCS, the mobilized concrete fracture surface surrounding the FRP strips should be as maximum as possible, which is attained by maximizing the following effective element width factor (b_e):

$$b_e = 2.s_c.N \le b \tag{18}$$

where b is the width of the beam's cross section (Fig. 2).

In this regard, although a negative value of y_c leads to a bending moment impeding the CCS failure to initiate at the FRP end section (see Fig. 5), the tensile fracture of the concrete cover at this FRP end section can occur due to the FRP tensile force (F_f) in the longitudinal direction of the FRP.

The effective concrete fracture capacity (F_{fe}) of the FRP strips can be determined by summing the concrete fracture capacity ($F_{f(\max)}$) of all the FRP strips flexurally applied on the tensile surface of the beam:

$$F_{fe} = \sum_{i=1}^{N} F_{f(\max)i} \tag{19}$$

where N is the number of the NSM FRP reinforcements.

Considering this effective concrete fracture capacity (F_{fe}) of the FRP strips, the flexural capacity (M_{CCS}^{Lrb}) of the strengthened beam at the end section of the resisting bond length (L_{rb}) can be obtained by Eq. (20), where the beam's cross section is supposed to be in a loading stage between those corresponding to the concrete cracking and steel yield initiation phases (postcracking stage). In this regard, the compressive behavior of concrete is assumed linear up to the yielding of the longitudinal tensile steel reinforcement in order to simplify the calculation procedure. Otherwise, for the section in the postyielding stage, the contribution of concrete in compression should be simulated by a rectangular compressive stress block recommended by ACI-440 [1], and the compressive and tensile stresses in the longitudinal top and bottom steel bars, respectively, should be limited by its yield strength ($f_{sy} = \varepsilon_{sy}.E_s$).

$$M_{CCS}^{Lrb} = \frac{1}{3}\varepsilon_{cc,CCS}.E_c.b.c_{CCS}^2 + \varepsilon_{s,CCS}^{'}.E_s.A_s^{'}.\left(c_{CCS} - d_s^{'}\right) + \varepsilon_{s,CCS}.E_s.A_s.\left(d_s - c_{CCS}\right) + F_{fe}.\left(d_f - c_{CCS}\right) \tag{20}$$

in which E_c and E_s are the elasticity modulus of concrete and steel reinforcement, respectively; $d_s^{'}$, d_s , and d_f are the internal arm of top and bottom longitudinal steel bars and FRP reinforcement, respectively; $A_s^{'}$ and A_s are the cross sectional area of top and bottom longitudinal steel bars; ε_{sy} is the strain corresponding to the steel tensile yield strength. Moreover, the strains of the constituent materials along the cross section can be determined adopting the proportional strain distribution to the distance from the neutral axis depth (c_{CCS}) by considering the average tensile strain in the FRP strips ($\varepsilon_{fe} = F_{fe} / (N.a_f.b_f.E_f)$), (see Appendix B).

According to the principles of static equilibrium and proportionality of the strain distribution along the cross section, the neutral axis depth (c_{CCS}) at the end section of resisting bond length (L_{rb}) can be obtained using a quadratic equation represented in Eq. (21) (Appendix B).

$$a.c_{CCS}^2 + b.c_{CCS} + c = 0 \tag{21a}$$

where

$$\begin{aligned} a &= E_c.b \\ b &= 2.\left(E_s.A_s^{'} + E_s.A_s + E_f.N.a_f.b_f\right) \\ c &= -2.\left(E_s.A_s^{'}.d_s^{'} + E_s.A_s.d_s + E_f.N.a_f.b_f.d_f\right) \end{aligned} \tag{21b}$$

As a final point, the ultimate flexural capacity (M_{CCS}^u) of the NSM FRP strengthened beam, adopting the concrete cover separation as the prevailing failure mode at ultimate stage, is determined according to the bending moment distribution along the beam length considering the corresponding loading configuration. For instance, regarding to the simply supported beam subjected to a four-point monotonic loading configuration (the adopted one in the current analytical study), M_{CCS}^u is determined by the following equation (Fig. 6).

$$M_{CCS}^u = \frac{b_s.M_{CCS}^{Lrb}}{(L_{rb} + L_{ub})} \tag{22}$$

where b_s is the distance between the support and the nearest point load (shear span) and L_{ub} is the length of unstrengthened shear span (the distance between the support and the end of the FRP strip bonded length), see Fig. 4.

3. Assessment of the predictive performance of the analytical approach

The performance of the described analytical approach is assessed by predicting the ultimate flexural capacity of the NSM FRP strengthened beams that failed with concrete cover separation. The model was applied to fifteen NSM CFRP strengthened beams tested by Sharaky (2014), Sharaky et al. (2015), Al-Mahmoud et al. (2009), Barros and Fortes (2005), Barros et al. (2007), Bilotta et al. (2015), Jumaat et al. (2015), Teng et al. (2006), and Sena-Cruz et al. (2012) [15-23]. The geometry, support, and loading conditions of the tested beams are represented schematically in Fig. 2, and the corresponding data is included in Table 1. Moreover, Table 2 provides the steel and CFRP reinforcement details of these tested beams. The main material properties of the beams are indicated in Table 3. A relatively high shear reinforcement ratio was adopted for all the beams in order they do not fail in shear.

The parameters of the local bond-slip relationship for all the tested beams were adopted similar to the corresponding values considered by [13]: $\tau_{\max} = 20.1\,\text{MPa}$ and $\delta_{\max} = 7.12\,\text{mm}$ (Fig. 3b). Furthermore, the angle (α) between the FRP longitudinal axis and generatrices of the semi-pyramidal part of concrete fracture body for all the analyzed beams was determined using an empirical formula defining the relationship between this fracture angle and the boundary limits of the concrete fracture body adopted for the tested beams. These boundary limits were considered adopting s_c parameter obtained by Eq. (5). Regarding this empirical formula, first the fracture angle (α) was obtained for each analyzed beam using a back analysis of the experimental data by fitting as better as possible the ultimate flexural capacity developing the CCS failure. In this regard, Fig. 7a shows the relationship between these angles and corresponding s_c of the analyzed beams. Next, a formula was proposed, using the best fitted curve of the data represented in Fig. 7a, to obtained the fracture angle (α) for the NSM FRP strengthened beams considering the boundary limits of the concrete fracture body, as follows:

$$\alpha = 618.84\, s_c^{-0.94} \quad for \quad s_c \leq b/2 \tag{23}$$

For current values of s_c, around 25 mm, the angle is close to the value proposed by [13], 28 degrees, which is an extra support for the confidence of Eq. (23), but further research is this respect should be carried out. In fact, this formulation was calibrated mainly considering the cases of RC beams strengthened using CFRP composite materials, therefore for the cases of RC beams strengthened with FRP composite materials other than CFRP, the Eq. (23) should be recalibrated considering the relevant experimental data. The ultimate flexural capacity obtained analytically and registered experimentally for all the tested beams is compared in Fig. 7b. Moreover, Table 4 represents the ratio between the analytical and experimental flexural capacity of the analyzed beams when failing by concrete cover separation, where a good predictive performance is evidenced for the proposed analytical approach considering the average value of 1.0 with a standard deviation of 0.16. This table also indicates the comparison between the concrete tensile fracture capacity ($F_{f\,(\max)}$) with the tensile strength of CFRP (F_{fu}) and resisting bond force (F_{rb}) corresponding to the resisting bond length (L_{rb}) for each NSM CFRP. Since all these beams have failed by CCS, the $F_{f\,(\max)}$ was the minimum value amongst the three components.

Beside the CCS failure of beams strengthened with NSM FRPs, the experimental tests evidenced that the intermediate crack (IC) debonding failure can be also expected as a premature failure before the conventional flexural failure modes [24]. The IC debonding failure starts from the flexural/shear cracks within the shear span and propagates towards the NSM FRPs termination, while the CCS failure initiates by cracks at the FRP-end section and horizontally propagates towards the maximum bending moment zone [24, 25].

On this subject, Oehlers et al. (2008) proposed a mathematical model for the IC debonding resistance of NSM FRPs applied for the flexural strengthening of RC beams. Concerning the occurrence of this IC failure before or after the CCS failure in the NSM FRP RC beams, Table 4 compares analytically the load carrying capacity, corresponding to the IC and CCS failures, of the analyzed strengthened beams, where the relevant IC capacities were determined using the proposed model by [25]. This table evidences a lower load carrying capacity at the CCS failure compared to the corresponding capacity at the IC failure for the analyzed beams.

4. Parametric study

By using the developed analytical model, parametric studies were carried out to evaluate the influence of the relevant parameters of the model on the maximum flexural capacity of RC structures failing by CCS failure. The parameters adopted in this parametric study were of the following ones: 1) material properties: the concrete compressive strength, and the elasticity modulus of FRP; 2) FRP strengthening configuration: FRP bonded length, NSM FRP installation depth from the tensile surface of the RC element, distance between consecutive NSM FRPs, and number of NSM FRP reinforcements.

For this purpose, the experimental program composed of RC beams strengthened with NSM CFRP strips conducted by [20] was adopted for the parametric study, and the geometric data and main material properties of these beams are indicated in Tables 1-3. The CCS failure capacity obtained analytically using the proposed model for this experimental program was 32.8 kN (see Table 4) and in this parametric study, by varying the aforementioned parameters, the obtained CCS failure capacities were normalized (divided by) to this failure capacity (32.8 kN). For facilitating the comparison between the influences of the adopted parameters on the CCS failure capacity, the adopted values for these parameters were normalized to the corresponding ones in the experimental program. Moreover, in this regard, an equal variation ratio (0.5, 1, and 1.5) was used for all the parameters considering the accessible values in field strengthening applications.

4.1. Material properties

Regarding to the parametric study in terms of material properties, Figs. 8a and 8b show the influence of the normalized concrete compressive strength ($f_c^{'}/f_c^{'analy}$) and FRP elasticity modulus (E_f/E_f^{analy}) on the normalized CCS failure capacity (F_{CCS}/F_{CCS}^{analy}), where normalized means that the CCS failure capacity is divided by the CCS analytical capacity of the strengthened beam conducted by [20] and designated by F_{CCS}^{analy}. This figure evidences that by increasing the concrete compressive strength, the CCS failure capacity of the structures increases due to the higher resistance provided by the surrounding concrete at the extremities of NSM FRPs. However, the CCS failure capacity decreases with the increase of FRP elasticity modulus, since a higher FRP elasticity modulus results in a lower average tensile strain in the FRP reinforcement (ε_{fe}) at the end section of resisting bond length (L_{rb}) (considering a constant value for F_{fe}), causing a lower bending moment capacity (M_{CCS}^{Lrb}) at this section due to the smaller strain distribution along the section.

4.2. FRP strengthening configuration

In order to analytically evaluate the influence of FRP strengthening configuration on the CCS failure capacity, Figs. 9a and 9b compare the influence of the normalized length of unstrengthened shear span (L_{ub}/L_{ub}^{analy}) and NSM FRP installation depth from the tensile surface of the RC element (l_f/l_f^{analy}) on the CCS failure capacity (Fig. 2). Fig. 9 shows that the CCS failure capacity decreases with the increase of the length of unstrengthened shear span according to the Eq. (22). Moreover, installing the NSM FRP more far away from the tensile surface of the RC element results in a higher CCS failure capacity, since the vertical eccentricity (y_c) of the FRP tensile force (F_f) to the centroid of the concrete fracture body reduces, causing a lower active moment ($M_f = F_f . y_c$) and a higher CCS failure capacity according to the Eq. (16). In this regard, Fig. 9b also evidences that adopting l_f/l_f^{analy} of 1.5 caused a negative value for the vertical eccentricity of the FRP tensile force ($y_c < 0$), and consequently, the occurrence of the CCS failure by crack initiation at the FRP end section is impossible.

In the next stage of the current parametric study, FRP strengthening configuration in terms of the number of NSM FRPs and distance between consecutive FRPs is analytically evaluated using the developed model. Fig. 10a shows the influence, on the normalized CCS failure capacity, of the ratio between the distance from the beam edge and nearest NSM FRP ($s_f^{'}$) and two adjacent NSM FRPs (s_f), $s_f^{'}/s_f$. In this regard, the $s_f^{'}/s_f$ ratio adopted in the analyzed experimental tests was almost 1.5, as represented in Table 2 and C1 configuration in Fig. 10. Moreover, Table 5 indicates the main relevant results regarding the influence of the $s_f^{'}/s_f$ ratio on the normalized CCS failure capacity. This table evidences that the CCS failure capacity increases by a higher ratio between the effective width (b_e) and width (b) of element (b_e/b). The maximum increase of this b_e/b ratio is obtained by adopting the $s_f^{'}/s_f$ ratio equals to 0.5 (configuration C2 in Fig. 10), causing $b_e/b = 1$ (see Table 5). In fact, when $s_f^{'}/s_f = 0.5$ an increase of about 120% in terms of the CCS failure capacity is obtained when compared to the corresponding capacity determined analytically for the adopted experimental beams with distance ratio of $s_f^{'}/s_f = 1.5$.

On the other hand, Fig. 10b represents the effectiveness of NSM FRP configuration in terms of the number of NSM FRPs (N) on the normalized CCS failure capacity. For this purpose, the NSM CFRP configurations C3 (with two strips of 2.1×10 (2S: 2.1×10)) and C4 (with a strip of 4.2×10 (1S: 4.2×10)) are adopted with the aim of providing a NSM CFRP reinforcement ratio equal to the one adopted in the experimental beam tests (configuration C1 with three strips of 1.4×10 (3S: 1.4×10)) (see Fig. 10). Furthermore, the main relevant results derived from Fig. 10b are represented in Table 6. This table evidences that, by decreasing the number of NSM FRP reinforcements, the CCS failure capacity is significantly increased, as long as the adopted FRP configurations satisfy $b_e/b=1$, which happened for the configurations C2 and C3. However, when the number of NSM FRP reinforcements decreases, and the width ratio (b_e/b) becoming less than 1 ($b_e/b<1$), the CCS failure capacity decreases, which is the case of C4 configuration. Accordingly, to increase the strengthening effectiveness under the framework of avoiding the occurrence of CCS, the number of NSM FRPs should be minimized with $s'_f/s_f=0.5$ considering maximizing the width ratio (b_e/b).

5. Conclusion

In the current study, a novel simplified analytical approach, with a design framework, was developed for the prediction of the maximum flexural capacity of RC structures strengthened using FRP reinforcement according to NSM technique failing by concrete cover separation (CCS) initiated at the end section of the NSM FRPs. This analytical approach was developed based on a closed form solution with the aim of being a guideline for designers. The good predictive performance of the analytical approach was evidenced by predicting the ultimate flexural capacity of fifteen NSM CFRP strengthened beams failed by CCS failure. Then, a series of parametric studies was analytically carried out using the developed model with the aim of proposing some design recommendations in this regard, as follows:

- By increasing the concrete compressive strength, the CCS failure capacity of the strengthened structures increases, while the opposite occurs with the increase of the FRP elasticity modulus.
- The CCS failure capacity is enhanced with the increase of the NSM FRP bonded length of the strengthened structure. Hence, in real applications, for design strengthening purposes, the extremities of the NSM FRPs should terminate as closest as possible to the support of the beam.
- Installing the NSM FRP as far away as possible from the tensile surface of the structure results in a higher CCS failure capacity.

- FRP strengthening configuration in terms of the adopted distances between two adjacent NSM FRPs (s_f) and from the beam edge to the nearest NSM FRP ($s_f^{'}$) has a noticeable effect on the CCS failure capacity. The $s_f^{'}/s_f$ ratio equals to 0.5 can minimize the detrimental interaction between the consecutive NSM FRPs, resulting in a higher CCS failure capacity for the NSM FRP strengthened structures.
- By decreasing the number of NSM FRP reinforcements, the CCS failure capacity is significantly increased, as long as the adopted FRP configurations provide the utilization of a mobilized concrete fracture surface surrounding the extremities of FRP strips with a total width (b_e) in the concrete substrate equals to the width of the beam's cross section (b). Accordingly, to increase the strengthening effectiveness under the framework of avoiding the occurrence of CCS, the number of NSM FRPs should be minimized with $s_f^{'}/s_f = 0.5$ considering maximizing the width ratio (b_e/b).

6. Acknowledgement

The authors acknowledge the financial support provided by QREN (through the Operational Program COMPETE) in the scope of the CutInov Project (n. 38780) involving the Clever Reinforcement Company and the Structural Composites Research group of ISISE-Minho University.

NOTATIONS

The following symbols are used in this paper:

A_c	:	cross sectional area of surrounding concrete, mm^2.
A_f	:	area of FRP reinforcement, mm^2.
A_s	:	area of tensile steel bars, mm^2.
$A_s^{'}$	:	area of compressive steel bars, mm^2.

a_f	:	thickness of FRP strip, mm.
a_L	:	loading span, mm.
b	:	width of beam, mm.
b_e	:	effective element width factor, mm.
b_f	:	height of FRP strip, mm.
b_s	:	shear span, mm.
c	:	depth of neutral axis from top fiber of concrete, mm.
c_c	:	concrete cover thickness beneath the longitudinal tensile steel bars, mm.
d_s	:	distance from centroid of tensile steel bars to top fiber of concrete, mm.
$d_s^{'}$	:	distance from centroid of compressive steel bars to top fiber of concrete, mm.
d_f	:	distance from centroid of FRP reinforcement to top fiber of concrete, mm.
E_c	:	elasticity modulus of concrete, MPa.
e_c	:	epoxy cover thickness beneath the FRP strip, mm.
E_f	:	elasticity modulus of FRP, MPa.
E_f^{analy}		elasticity modulus of FRP adopted analytically for the beam of [20], MPa.
E_s	:	elasticity modulus of longitudinal steel bars, MPa.
$f_c^{'}$	:	specified compressive strength of concrete, MPa.
$f_c^{'analy}$	:	compressive strength of concrete adopted analytically for the beam of [20], MPa.
F_{CCS}		CCS failure capacity, N.
F_{CCS}^{analy}		CCS failure capacity obtained analytically for the beam of [20], N.
f_{ct}	:	splitting tensile strength of concrete, MPa.
$f_{ct}(x)$	:	concrete tensile with respect to the corresponding concrete tensile strength, MPa.
F_{ctv}	:	vertical tensile resistance of concrete on top slant area, N.

F_f : FRP tensile force, N.

F_{fe} : effective concrete fracture capacity, N.

$F_{f(\max)}$: resistance of the concrete fracture surface for each FRP strip, N.

f_{fu} : tensile strength of FRP, MPa.

F_{rb} : maximum value of the force transferable through the resisting bond length, N.

F_{rbe} : maximum debonding resistance, N.

f_{sy} : yield strength of longitudinal tensile steel bar, MPa.

L : structure span, mm.

L_b : bonded length of FRP reinforcement, mm.

L_{be} : effective resisting bond length, mm.

l_f : FRP installation depth, mm.

l_f^{analy} : FRP installation depth adopted analytically for the beam of [20], mm.

L_{rb} : resisting bond length, mm.

l_s : slant length of the side faces of the concrete fracture body, mm.

l_t : slant length of the top face of the concrete fracture body, mm.

L_{ub} : length of unstrengthened shear span, mm.

L_{ub}^{analy} : length of unstrengthened shear span adopted analytically for the beam of [20], mm.

M_{CCS}^{Lrb} : flexural moment of structure at the end section of resisting bond length, N-mm.

M_{CCS}^{u} : maximum flexural moment of structure failing by CCS, N-mm.

M_f : FRP active moment, N-mm.

M_r : concrete resistant moment, N-mm.

N : number of the longitudinal FRP strip.

$N.A.$: neutral axis of structure.

s_c	:	limitation for concrete fracture body, mm.
s_f	:	spacing of the two adjacent FRP strips, mm.
$s_f^{'}$	:	distance between the structure edge and the nearest strip, mm.
T_s	:	vertical shear resistance of concrete on the side faces, N.
y_c	:	vertical eccentricity of FRP tensile force to the centroid of fracture shape, mm.
α	:	angle between axis and generatrices of the concrete fracture surface (semi-pyramid).
$\delta_{\max}$	:	maximum slip of local bond stress-slip relationship, mm.
ε_{cc}	:	strain level in concrete, mm/mm.
ε_{fe}	:	average tensile strain of FRP reinforcement, mm/mm.
ε_s	:	strain in longitudinal tensile steel bar, mm/mm.
$\varepsilon_s^{'}$	:	strain in longitudinal compressive steel bar, mm/mm.
ε_{sy}	:	strain in longitudinal tensile steel bars corresponding to its yield strength, mm/mm.
$\tau_{\max}$	:	maximum shear stress of local bond stress-slip relationship, MPa.
τ_s	:	concrete shear strength, MPa.
$\tau_s(x)$	:	shear stresses with respect to the corresponding concrete shear strength, MPa.

APPENDIX A

In order to obtain the vertical eccentricity (y_c) of the FRP tensile force (F_f) to the centroid of the concrete fracture body, this fracture body is divided by two semi-pyramidal and wedge parts. The vertical position of the centroid of the semi-pyramidal part (y_{cp}) can be obtained using Eq. (A1) (Fig. A1).

$$y_{cp}=\int_0^{Lrb}\left(A_{(x)}.y_{cp(x)}/V_{cp}\right).dx=\int_0^{Lrb}\left(\left(2.s_{c(x)}.s_{c(x)}\right).\left(s_{c(x)}/2\right)/V_{cp}\right).dx=3.s_c/8$$

where

$$s_{c(x)}=\left(s_c/L_{rb}\right).x$$

$$V_{cp}=\int_0^{Lrb}A_{(x)}.dx=\int_0^{Lrb}\left(2.s_{c(x)}.s_{c(x)}\right).dx=2.s_c^2.L_{rb}/3 \tag{A1}$$

On the other side, the vertical position of the centroid of the wedge part (y_{cw}) is determined as follows (Fig. A1):

$$y_{cw}=\int_0^{Lrb}\left(A_{(x)}.y_{cw(x)}/V_{cw}\right).dx=\int_0^{Lrb}\left(\left(2.s_{c(x)}.l_f\right).\left(l_f/2\right)/V_{cw}\right).dx=l_f/2$$

where

$$s_{c(x)}=\left(s_c/L_{rb}\right).x$$

$$V_{cw}=\int_0^{Lrb}A_{(x)}.dx=\int_0^{Lrb}\left(2.s_{c(x)}.s_{c(x)}\right).dx=s_c.L_{rb}.l_f \tag{A2}$$

Finally, the vertical eccentricity (y_c) of the FRP tensile force (F_f) to the centroid of the concrete fracture body can be obtained by:

$$y_c=\left(y_{cp}.V_{cp}-y_{cw}.V_{cw}\right)/\left(V_{cp}+V_{cw}\right)=\left(3.s_c^2-6.l_f^2\right)/\left(8.s_c+12.l_f\right) \tag{A3}$$

APPENDIX B:

By adopting the principles of static equilibrium of the beam's cross section located in the postcracking stage at the end section of resisting bond length (L_{rb}) (Fig. A2):

$$\frac{1}{2}\varepsilon_{cc,CCS}\,E_c.c_{CCS}.b+A_s^{'}.\varepsilon_{s,CCS}^{'}.E_s-A_s.\varepsilon_{s,CCS}.E_s-A_f.\varepsilon_{fe}.E_f=0 \tag{B1}$$

where strains at the top fiber of concrete (ε_{cc}) and longitudinal top ($\varepsilon_s^{'}$) and bottom (ε_s) steel bars can be obtained by:

$$\varepsilon_{cc,CCS}=\frac{\varepsilon_{ef}.c_{CCS}}{\left(d_f-c_{CCS}\right)} \tag{B2}$$

$$\varepsilon_{s,CCS}^{'} = \frac{\varepsilon_{ef}.\left(c_{CCS} - d_s^{'}\right)}{\left(d_f - c_{CCS}\right)} \leq \varepsilon_{sy} \quad \text{(B3)}$$

$$\varepsilon_{s,CCS} = \frac{\varepsilon_{ef}.\left(d_s - c_{CCS}\right)}{\left(d_f - c_{CCS}\right)} \leq \varepsilon_{sy} \quad \text{(B4)}$$

By substituting Eqs. (B2)-(B4) into Eq. (B1) yields:

$$\frac{1}{2}\left(\frac{\varepsilon_{ef}.c_{CCS}}{\left(d_f - c_{CCS}\right)}\right)E_c.c_{CCS}.b + A_s^{'}.\left(\frac{\varepsilon_{ef}.\left(c_{CCS} - d_s^{'}\right)}{\left(d_f - c_{CCS}\right)}\right).E_s - A_s.\left(\frac{\varepsilon_{ef}.\left(d_s - c_{CCS}\right)}{\left(d_f - c_{CCS}\right)}\right).E_s - A_f.\varepsilon_{fe}.E_f = 0 \quad \text{(B5)}$$

By rewiring Eq. (B5), Eq. (B6) is obtained to calculate the neutral axis depth (c_{CCS}) at this postcracking stage:

$$\left(E_c.b\right).c_{CCS}^2 + 2.\left(E_s.A_s^{'} + E_s.A_s + E_f.N.a_f.b_f\right).c_{CCS} - 2.\left(E_s.A_s^{'}.d_s^{'} + E_s.A_s.d_s + E_f.N.a_f.b_f.d_f\right) = 0 \quad \text{(B6)}$$

7. References

[1] ACI-440-2R. Guide for the design and construction of externally bonded FRP systems for strengthening concrete structures. American Concrete Institute (ACI), 2008.

[2] Sas G, Dăescu C, Popescu C, Nagy-György T. Numerical optimization of strengthening disturbed regions of dapped-end beams using NSM and EBR CFRP. Composites Part B: Engineering, 2014; 67. pp: 381-390.

[3] Rezazadeh M, Costa I, Barros J. Influence of prestress level on NSM CFRP laminates for the flexural strengthening of RC beams. Composite Structures. 2014;116:489-500.

[4] Jiang S-F, Zeng X, Shen S, Xu X. Experimental studies on the seismic behavior of earthquake-damaged circular bridge columns repaired by using combination of near-surface-mounted BFRP bars with external BFRP sheets jacketing. Engineering Structures. 2016;106:317-31.

[5] Kotynia R, Lasek K, Staskiewicz M. Flexural Behavior of Preloaded RC Slabs Strengthened with Prestressed CFRP Laminates. Journal of Composites for Construction (ASCE). 2013;18:A4013004.

[6] Barros J, Kotynia R. Possibilities and challenges of NSM for the flexural strengthening of RC structures. The 4th International Conference on FRP Composites in Civil Engineering (CICE 2008), Zurich, Switzerland, 2008.

[7] Costa I, Barros J. Flexural and shear strengthening of RC beams with composite materials–The influence of cutting steel stirrups to install CFRP strips. Cement and Concrete Composites. 2010;32:544-53.

[8] Rezazadeh M, Barros J, Costa I. Analytical approach for the flexural analysis of RC beams strengthened with prestressed CFRP. Composites Part B: Engineering. 2015;73:16-34.

[9] Zhang S, Teng J. Finite element analysis of end cover separation in RC beams strengthened in flexure with FRP. Engineering Structures. 2014;75:550-60.

[10] Zhang S, Teng J. End cover separation in RC beams strengthened in flexure with bonded FRP reinforcement: simplified finite element approach. Materials and Structures. 2015:1-14.

[11] Rezazadeh M, Barros J. A new hybrid methodology according to near surface mounted carbon fiber reinforced polymer technique for the flexural strengthening of reinforced concrete beams. Journal of Reinforced Plastics and Composites. 2014;33:1993-2009.

[12] ACI-318-08. Building code requirements for structural concrete and commentary. American Concrete Institute (ACI); 2008.

[13] Bianco V, Monti G, Barros J. Design formula to evaluate the NSM FRP strips shear strength contribution to a RC beam. Composites Part B: Engineering. 2014;56:960-71.

[14] Bianco V, Barros J, Monti G. Three dimensional mechanical model for simulating the NSM FRP strips shear strength contribution to RC beams. Engineering Structures. 2009;31:815-26.

[15] Sharaky I. Theoretical Model and Computational Procedure to Evaluate the NSM FRP Strips Shear Strength Contribution to a RC Beam, PhD Thesis, University of Girona, Spain, 2014.

[16] Sharaky I, Torres L, Sallam H. Experimental and analytical investigation into the flexural performance of RC beams with partially and fully bonded NSM FRP bars/strips. Composite Structures. 2015;122:113-26.

[17] Al-Mahmoud F, Castel A, François R, Tourneur C. Strengthening of RC members with near-surface mounted CFRP rods. Composite Structures. 2009;91:138-47.

[18] Barros J, Fortes A. Flexural strengthening of concrete beams with CFRP laminates bonded into slits. Cement and Concrete Composites. 2005;27:471-80.

[19] Barros J, Dias S, Lima J. Efficacy of CFRP-based techniques for the flexural and shear strengthening of concrete beams. Cement and Concrete Composites. 2007;29:203-17.

[20] Bilotta A, Ceroni F, Nigro E, Pecce M. Efficiency of CFRP NSM strips and EBR plates for flexural strengthening of RC beams and loading pattern influence. Composite Structures. 2015;124:163-75.

[21] Jumaat M, Hosen M, Darain K, Obaydullah M. Innovative End Anchorage for Preventing Concrete Cover Separation of NSM Steel and CFRP bars Strengthened RC Beams. The 6th Jordanian International Civil Engineering Conference, Amman, Jordan, 2015.

[22] Teng J, De Lorenzis L, Wang B, Li R, Wong T, Lam L. Debonding failures of RC beams strengthened with near surface mounted CFRP strips. Journal of Composites for Construction (ASCE). 2006;10:92-105.

[23] Sena-Cruz J, Barros J, Coelho M, Silva L. Efficiency of different techniques in flexural strengthening of RC beams under monotonic and fatigue loading. Construction and Building Materials. 2012;29:175-82.

[24] Rezazadeh M, Cholostiakow S, Kotynia R, Barros J. Exploring new NSM reinforcements for the flexural strengthening of RC beams: Experimental and numerical research. Composite Structures. 2016141: 132-145.

[25] Oehlers D, Rashid R, Seracino R. IC debonding resistance of groups of FRP NSM strips in reinforced concrete beams. Construction and Building Materials. 2008;22.7: 1574-1582.

Table 1. Geometry, support, and loading conditions of the beams tested experimentally (dimensions in mm)

Tested beams	b (mm)	h (mm)	a_L (mm)	b_s (mm)	L_{ub} (mm)	$d_s^{'}$ (mm)	d_s (mm)	d_f (mm)	l_f (mm)	c_c (mm)
LB2S1+C1 beam of [15]	160	280	800	800	200	40	246	272	8	34
LB2S1+G1 beam of [15]	160	280	800	800	200	40	246	272	8	34
F2C1 beam of [16]	160	280	800	800	200	38	240	272	8	34
S-C6 (210-R) beam of [17]	150	280	1200	800	350	33	244	274	6	30
V2R2 beam of [18]	100	177	500	500	50	21	153	171	6	21
V3R2 beam of [18]	100	175	500	500	50	21	151	169	6	21
V4R3 beam of [18]	100	180	500	500	50	21	151	169	6	21
S2_NSM beam of [19]	120	170	300	300	50	21	149	162.5	7.5	19
S3_NSM beam of [19]	120	170	300	300	50	21	149	162.5	7.5	19
NSM_c_3 × 1.4 × 10_1 beam of [20]	120	160	250	925	100	30	115	152.5	7.5	40
NC12 beam of [21]	125	250	700	650	50	30	220	241	9	25
B500 beam of [22]	150	300	600	1200	1250	30	264	289	11	30
B1200 beam of [22]	150	300	600	1200	900	30	264	289	11	30
B1800 beam of [22]	150	300	600	1200	600	30	264	289	11	30
NSM beam of [23]	200	300	200	900	300	31	269	291.5	8.5	26

b and h: width and height of cross section, a_L and b_s: loading and shear spans, L_{ub}: the length of unstrengthened shear span, $d_s^{'}$, d_s, and d_f: internal arms of top and bottom steel bars and CFRP reinforcement, l_f: CFRP installation depth, c_c: concrete cover below the tensile steel bars

Table 2: Steel and CFRP reinforcement details of the beams tested experimentally

Tested beams	$A_s^{'}$ (mm)	A_s (mm)	ρ_s (%)	A_f (mm)	ρ_f (%)	s_f (mm)	$s_f^{'}$ (mm)	N_f
LB2S1+C1 beam of [15]	100.5	226.2	0.57	2S:1.4x20+1ϕ8	0.24	45.5	34.5	3
LB2S1+G1 beam of [15]	100.5	226.2	0.57	2S:1.4x20+1ϕ8*	0.17*	45.5	34.5	3
F2C1 beam of [16]	100.5	226.2	0.59	2ϕ8	0.23	80	40	2
S-C6 (210-R) beam of [17]	56.5	226.2	0.62	2ϕ6	0.14	88	31	2
V2R2 beam of [18]	100.5	84.8	0.55	2S:10x1.4	0.16	30	35	2
V3R2 beam of [18]	100.5	106.8	0.71	2S:10x1.4	0.16	30	35	2
V4R3 beam of [18]	100.5	150.8	0.89	3S:10x1.4	0.25	25	25	3
S2_NSM beam of [19]	66.3	66.4	0.37	2S:10x1.4	0.14	40	40	2
S3_NSM beam of [19]	66.3	99.5	0.55	3S:10x1.4	0.21	30	30	3
NSM_c_3 × 1.4 × 10_1 beam of [20]	157.1	157.1	1.14	3S:10x1.4	0.23	25	35	3
NC12 beam of [21]	157.1	226.2	0.82	2ϕ12	0.75	65	30	2
B500 beam of [22]	100.5	226.2	0.57	1S:2x16	0.07	150	75	1
B1200 beam of [22]	100.5	226.2	0.57	1S:2x16	0.07	150	75	1
B1800 beam of [22]	100.5	226.2	0.57	1S:2x16	0.07	150	75	1
NSM beam of [23]	157.1	235.6	0.43	4S:1.4 x 15	0.14	40	40	4

$A_s^{'}$, A_s, and A_f : area of top and bottom steel bars and CFRP reinforcement, ρ_s and ρ_f : steel and CFRP reinforcement ratios, s_f and $s_f^{'}$: distance of two adjacent CFRPs and distance between beam edge and nearest CFRP, N_f : number of NSM CFRPs, S: CFRP strip, ϕ: CFRP bar.

* This beam was flexurally strengthened using two CFRP strips and one GFRP bar and the relevant ρ_f was represented as an equivalent with respect to CFRP reinforcement.

Table 3: The mail material properties for concrete, steel and CFRP reinforcements

Tested beams	$f_c^{'}$ (MPa)	f_{sy} (MPa)	E_s (GPa)	f_{fu} (MPa)	E_f (GPa)
LB2S1+C1 beam of [15]	31.9	540	205	2350	170
LB2S1+G1 beam of [15]	31.9	540	205	CFRP:2350 GFRP: 1350	CFRP:170 GFRP: 64
F2C1 beam of [16]	30.5	540	200	2350	170
S-C6 (210-R) beam of [17]	36.7	600	210	1875	146
V2R2 beam of [18]	46	730	200	2740	159
V3R2 beam of [18]	46	730	200	2740	159
V4R3 beam of [18]	46	730	200	2740	159
S2_NSM beam of [19]	52.2	627	200	2740	159
S3_NSM beam of [19]	52.2	627	200	2740	159
NSM_c_3 × 1.4 × 10_1 beam of [20]	21	540	200	2052	171
NC12 beam of [21]	40	550	200	1861	127
B500 beam of [22]	44	532	210	2068	131
B1200 beam of [22]	44	532	210	2068	131
B1800 beam of [22]	44	532	210	2068	131
NSM beam of [23]	53	455	200	2435	158

$f_c^{'}$: concrete compressive strength, f_{sy}: steel yield strength, E_s and E_f: elasticity modulus of steel and FRP reinforcements, f_{fu}: CFRP tensile strength.

Table 4: Experimental and analytical values of the ultimate flexural capacity of the analyzed beams

Tested beams	s_c (mm)	y_c (mm)	α (°)	$F_{f(\max)}$ (kN)	F_{fu} (kN)	F_{rb} (kN)	F_{rbe} (kN)	F_{CCS}^{analy} (kN)	F_{CCS}^{exper} (kN)	$\frac{F_{CCS}^{analy}}{F_{CCS}^{exper}}$	F_{IC}^{analy} (kN)
LB2S1+C1 beam of [15]	22.8	4.2	33.0	7.1	83.2	13.1	117.0	126.0	119.7	1.05	211.8
LB2S1+G1 beam of [15]	22.8	4.2	33.0	7.1	61.1	11.2	94.5.0	157.0	120.7	1.30	223.2
F2C1 beam of [16]	26.0	5.4	28.9	10.5	118.1	20.9	153.4	115.0	117.2	0.98	127.9
S-C6 (210-R) beam of [17]	24.0	5.7	31.3	6.8	52.9	13.1	93.3	87.5	110.0	0.80	116.7
V2R2 beam of [18]	15.0	2.4	48.6	1.5	36.8	5.5	75.8	61.8	78.5	0.79	95.1
V3R2 beam of [18]	15.0	2.4	48.6	1.5	36.8	5.5	75.8	72.1	81.9	0.88	101.2
V4R3 beam of [18]	12.5	1.5	48.6	0.9	36.8	3.2	75.1	109.6	94.0	1.17	121.9
S2_NSM beam of [19]	11.5	0.3	62.3	2.7	36.8	3.4	76.5	111.7	92.5	1.21	164.5
S3_NSM beam of [19]	11.5	0.3	62.3	2.7	36.8	3.4	75.6	127.0	96.6	1.31	168.1
NSM_c_3 × 1.4 × 10_1 beam of [20]	12.5	0.7	57.6	1.4	28.7	3.3	81.2	32.8	33.3	0.98	35.6
NC12 beam of [21]	16.0	1.2	45.6	4.7	210.3	10.1	222.6	137.5	146.0	0.94	155.2
B500 beam of [22]	19.0	1.3	38.8	12.4	66.2	16.4	140.7	50.5	47.8	1.06	136.8
B1200 beam of [22]	19.0	1.3	38.8	12.4	66.2	16.4	140.7	70.9	63.1	1.12	136.8
B1800 beam of [22]	19.0	1.3	38.8	12.4	66.2	16.4	140.7	104.9	91.7	1.14	136.8
NSM beam of [23]	17.5	2.0	41.9	5.1	51.1	12.4	116.8	132.0	147.3	0.90	216.8

s_c: limitation for concrete fracture body, y_c: FRP force vertical eccentricity to the centroid of fracture shape, α: angle between axis and generatrices of the concrete fracture surface, $F_{f(\max)}$: resistance of the concrete fracture surface for each FRP strip, F_{fu}: ultimate tensile capacity of FRP, F_{rb}: maximum value of the force transferable through the resisting bond length, F_{rbe}: maximum debonding resistance, F_{CCS}^{analy}: CCS failure capacity obtained analytically, F_{CCS}^{exper}: CCS failure capacity obtained experimentally, F_{IC}^{analy}: IC failure capacity obtained analytically.

Table 5: The influence of the distance between consecutive NSM FRPs on the CCS failure capacity

s'_f/s_f	s_c *(mm)*	N	b_e/b	F_{CCS}/F_{CCS}^{analy}
0.25	16	3	0.8	1.90
0.5	20	3	1	2.21
1	15	3	0.75	1.16
1.5	12.5	3	0.62	1

Table 6: The influence of the number of NSM FRPs on the CCS failure capacity

FRP configuration	s'_f / s_f	s_c (mm)	N	b_e / b	$F_{CCS} / F_{CCS}^{analy}$
C1	1.5	12.5	3	0.62	1
C2	0.5	20	3	1	2.21
C3	0.5	30	2	1	4.21
C4	-	30	1	0.5	2.58

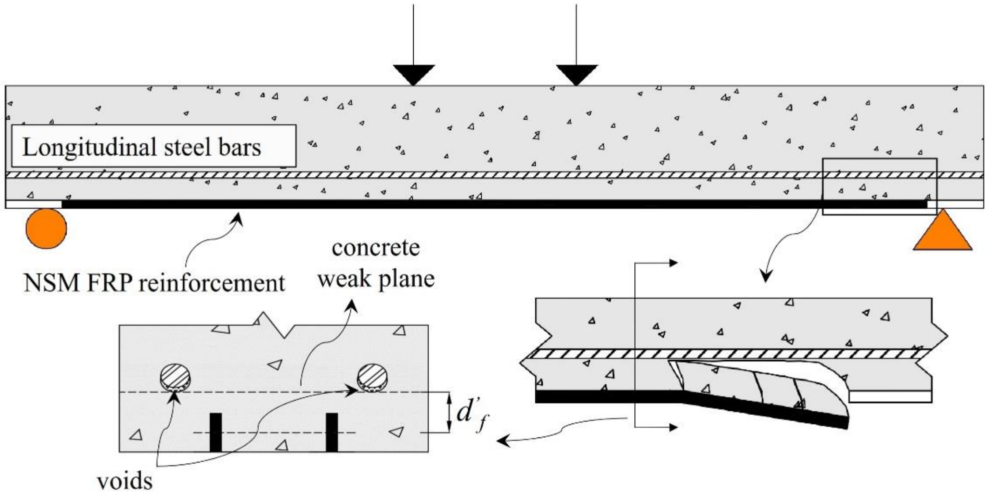

Fig. 1. Concrete cover separation of RC beams strengthened with NSM FRP reinforcement

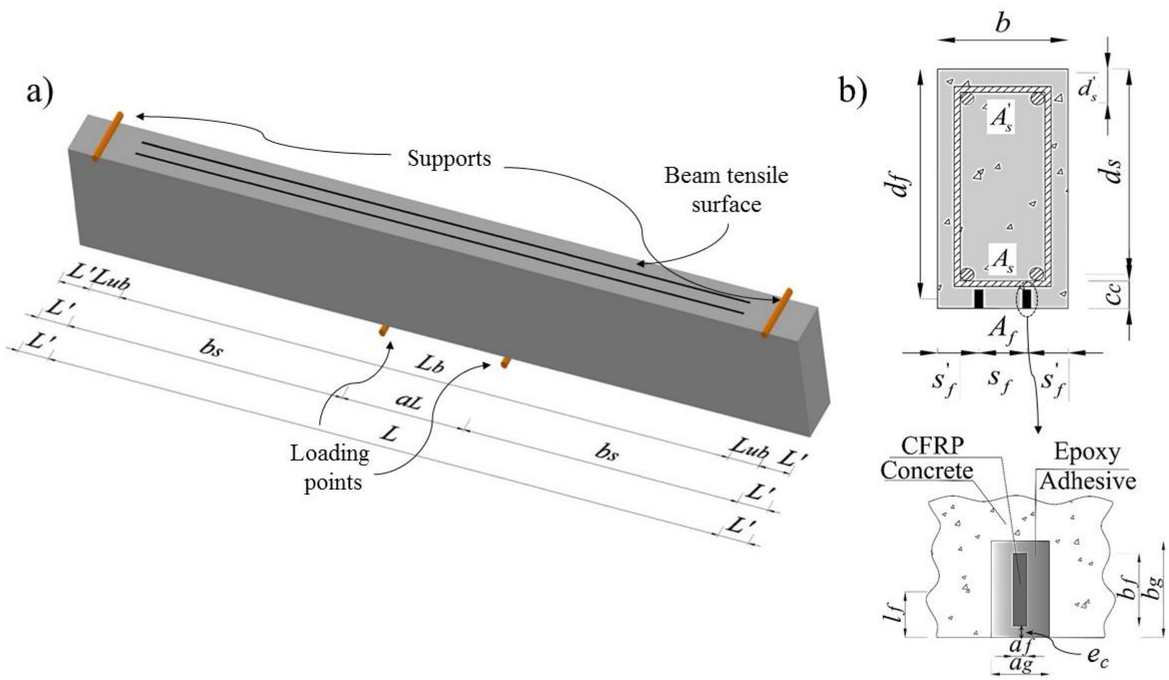

Fig. 2. Characteristics of NSM FRP strengthened beams: a) geometry, b) reinforcement details

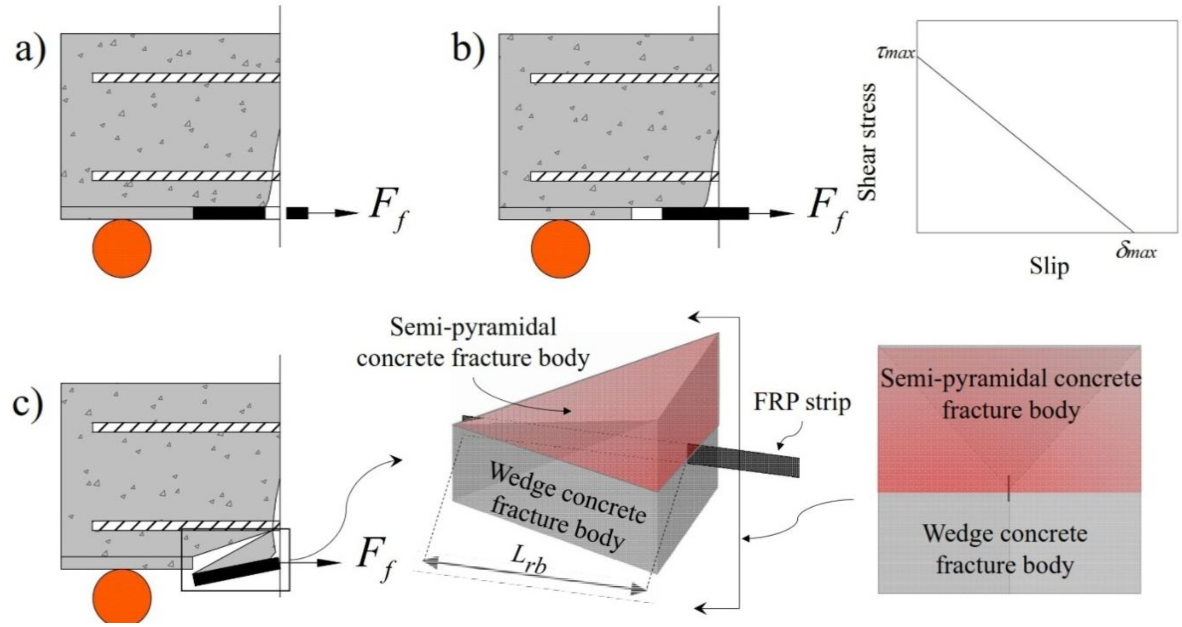

Fig. 3. Failure modes at the extremities of NSM FRP reinforcement: a) FRP rupturing, b) FRP debonding, c) concrete tensile fracture

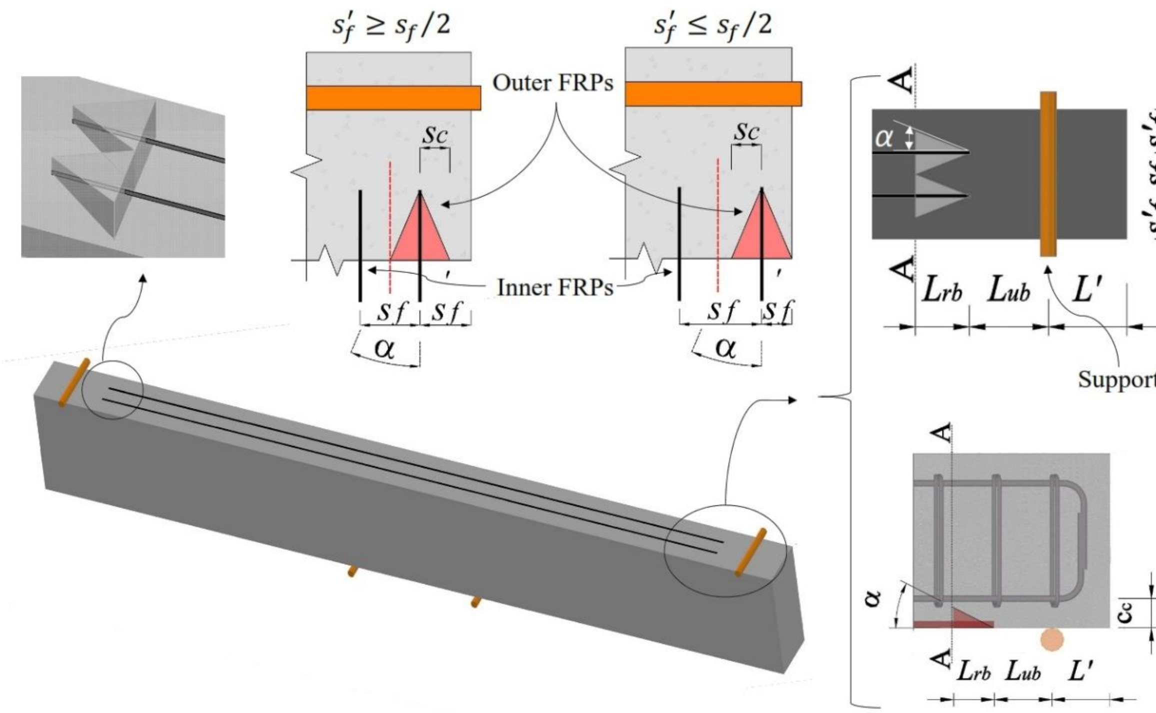

Fig. 4. Conditions assumed for the geometry of the concrete tensile fracture body at the extremities of NSM FRP reinforcement

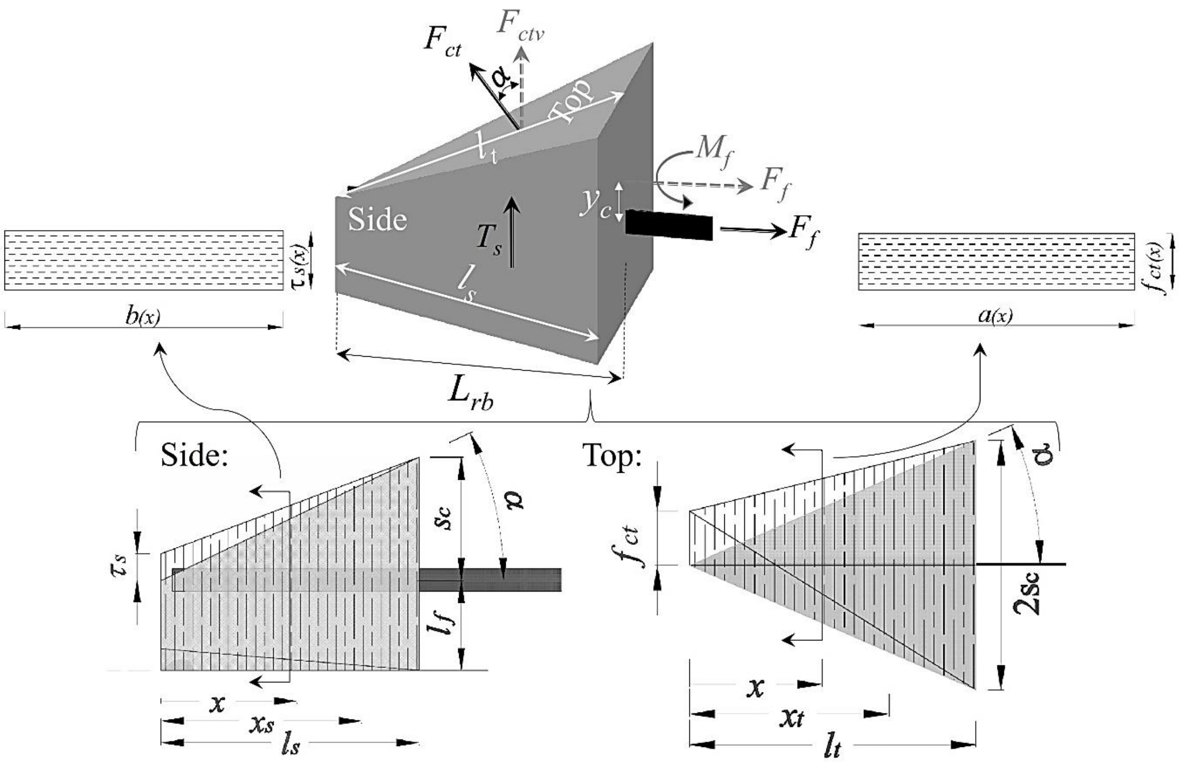

Fig. 5. Resistance of concrete tensile fracture body considering the tensile strength (on the top surface) and shear strength (on the side surfaces) of concrete

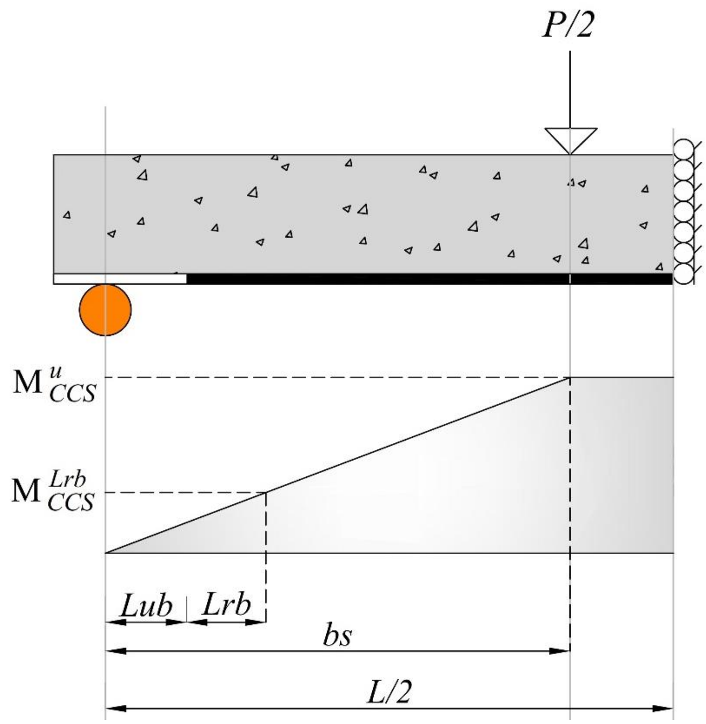

Fig. 6. Flexural bending moment distribution along the beam's length

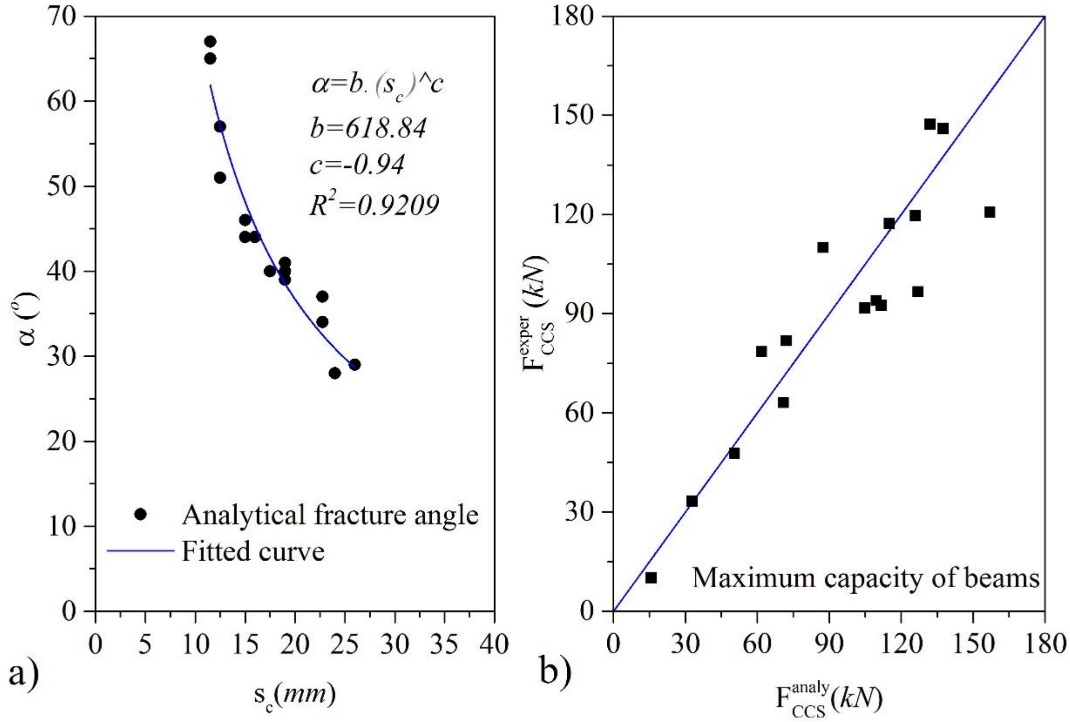

Fig. 7. a) Relationship of fracture angle versus relevant boundary limit, b) assessment of predictive performance of the analytical approach

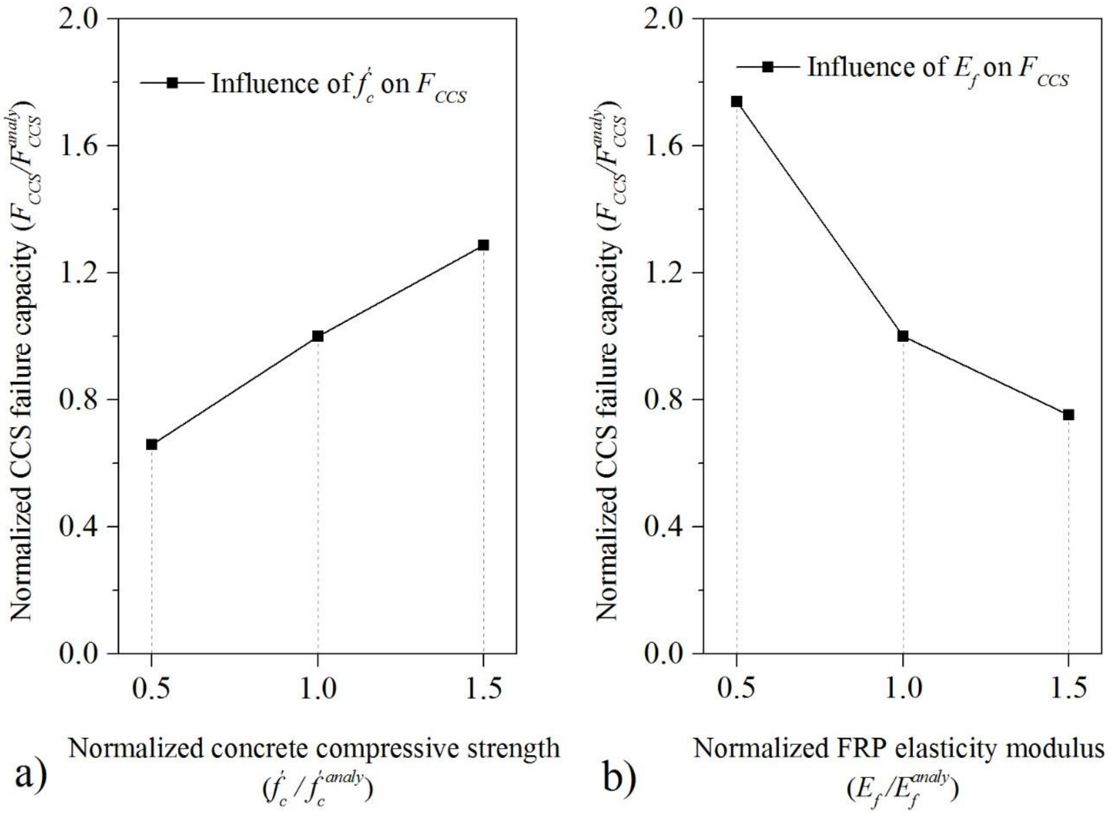

Fig. 8. The influence on the CCS failure capacity of: a) concrete compressive strength, b) FRP elasticity modulus

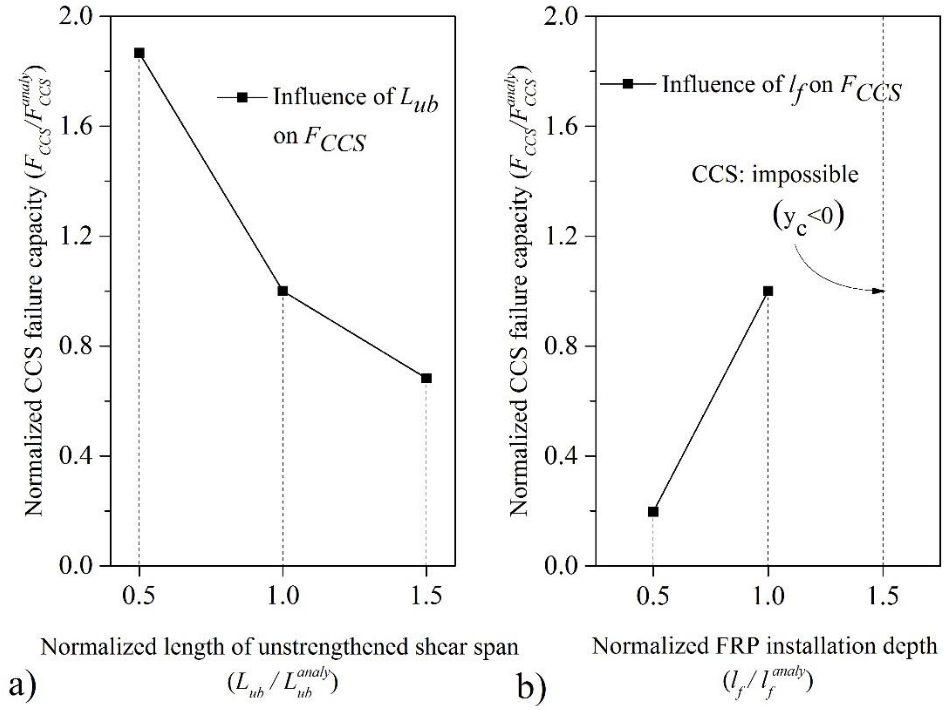

Fig. 9. The influence on the CCS failure capacity of: a) the length of unstrengthened shear span, b) FRP installation depth

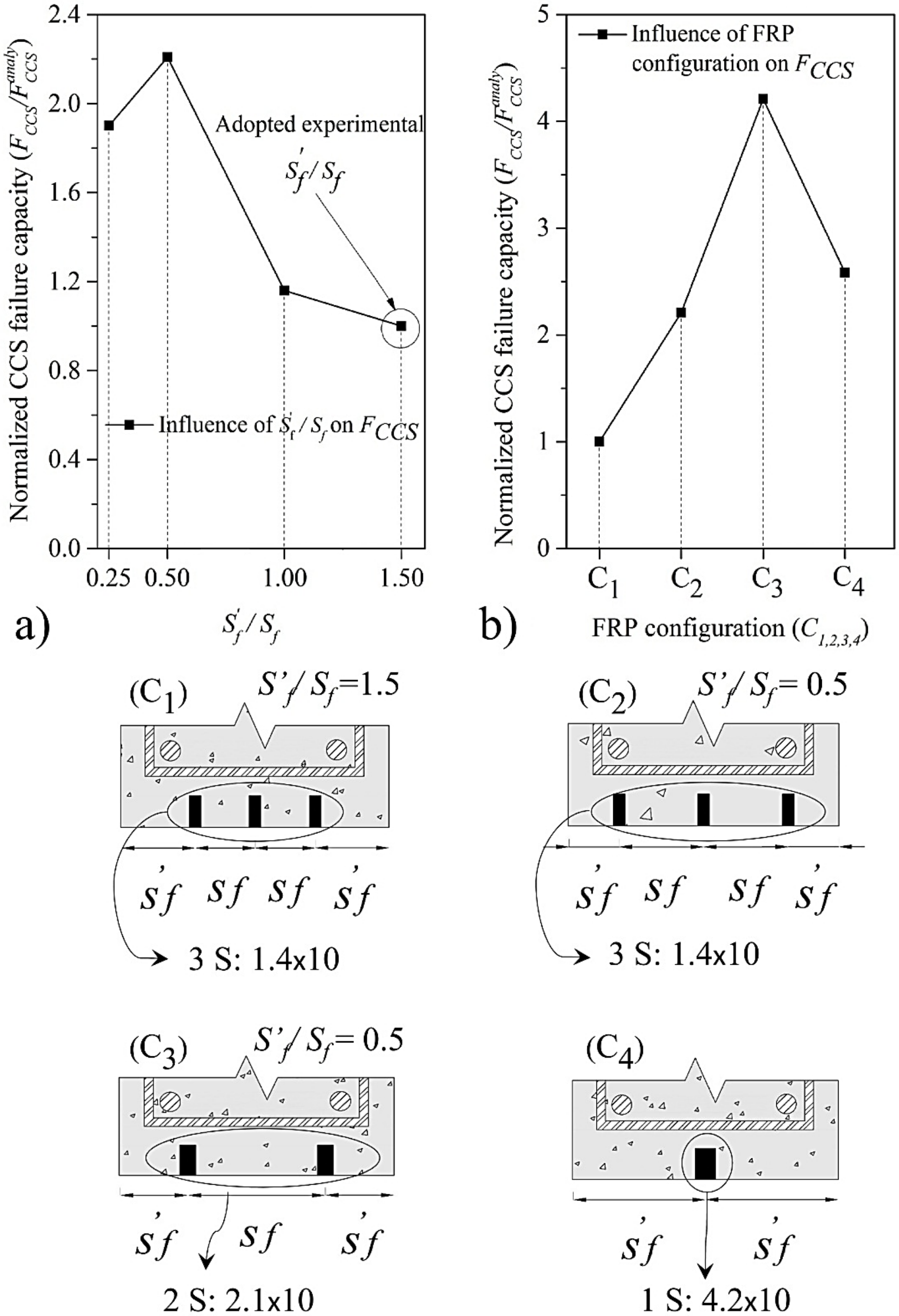

Fig. 10. The influence on the CCS failure capacity of: a) distance between the consecutive NSM FRPs, b) number of NSM FRPs

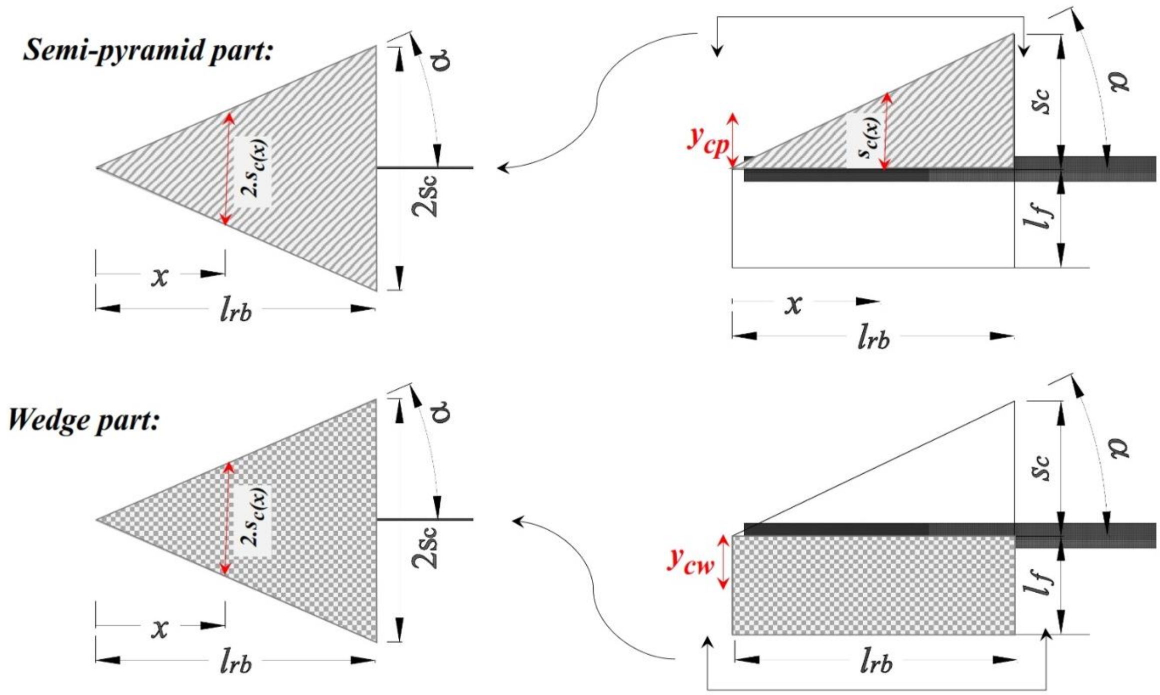

Fig. A1. The vertical position of the centroid of the semi-pyramidal and wedge parts of concrete fracture body

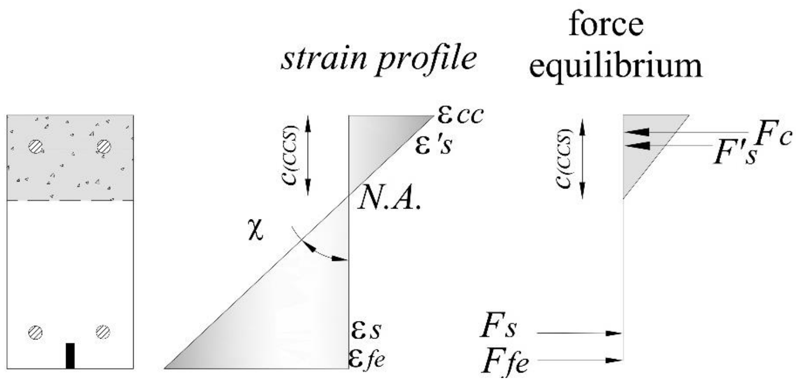

Fig. B1. Force equilibrium and strain distribution along the cross section at the end of resisting bond length